INSTITUTE OF PHYSICS PUBLISHING SEMICONDUCTOR SCIENCE AND TECHNOLOGY

Semicond. Sci. Technol. **17** (2002) 1004–1007 PII: S0268-1242(02)36785-3

Narrow-line light emission from porous silicon multilayers and microcavities

S H Xu, Z H Xiong, L L Gu, Y Liu, X M Ding, J Zi and X Y Hou

Surface Physics Laboratory (National Key Laboratory), Fudan University, Shanghai 200433, People's Republic of China

E-mail: xyhou@fudan.edu.cn

Received 9 May 2002, in final form 12 June 2002
Published 9 August 2002
Online at stacks.iop.org/SST/17/1004

Abstract

Porous silicon multilayers and microcavities, prepared by the pulsed electrochemical etching method, exhibit a variety of reflectivity and photoluminescence spectra. A comparison of the measured results with those calculated based on the transfer matrix method and quantum-box model reveals that the variation of the spectra can be attributed to the change in wavelength position of the stop-band of distributed Bragg reflectors and the maximum of the broad light emission of porous silicon. Different confined electric field modes appear in three different cases of porous silicon microcavities. Their different characteristics are summarized and considered as criteria to distinguish species of the porous silicon microcavities from their photoluminescence spectra.

1. Introduction

Recently, narrow-line light emission from porous silicon microcavities (PSMs) has attracted much attention [1–3]. Similar to a Fabry–Perot interference filter, a PSM consists of a layered structure with a central active medium (porous silicon (PSi) with a high porosity) sandwiched between two PSi distributed Bragg reflectors (DBRs). Narrow-line light emission can be acquired from such a structure by tailoring the emission characteristics of the PSi active layer. The emission is expected to appear at λ, the central wavelength of stop-band (plateau with high reflectance), if the central active medium consists of a λ or $\lambda/2$ PSi layer and the two dielectric multilayer mirrors are composed of alternating $\lambda/4$ PSi layers. But experimentally observed luminescence spectra of PSMs may actually vary from case to case. Instead of its appearance at the centre, the narrow-line light may also emit from the low/high wavelength cut-off of the stop-band. In addition, the PSi multilayer structure itself can also emit a narrow luminescence line [4]. In this paper, we sum up the experimental conditions to acquire various narrow-line light emissions of PSMs, and we systematically calculate the characteristics of various PSMs using the quantum-box model and the transfer matrix method (TMM) to clarify the experimental results. This may shed light on the origin of the different light emissions of PSMs and hence benefit the ultimate realization of PSi lasing in a layered PSi medium.

2. Experimental procedure and theoretical approach

The PSi multilayers and microcavities were prepared using PC-controlled pulsed electrochemical etching [6]. Heavily doped (∼0.01 Ω cm) p-type Si(001) wafers were chosen as the substrates and were electrochemically etched in a HF(48%):C_2H_5OH(99%):H_2O solution (1:1:2 by volume). The refractive index n of each layer formed was estimated by referring to a plot of n versus current [7], as was the thickness d, which was further checked by scanning electron microscopy [8]. Changes in the etching time and current density could thus be a control of d and n of the PSi DBRs and PSMs. In the present experiments, a shift of the bandgap was obtained by adjusting the thickness d of each PSi layer, with n remaining unchanged.

The samples were characterized by photoluminescence (PL) and reflectance analyses. The PL spectra were excited by the 441.6 nm line of a He–Cd laser, with a laser power of about 30 mW. The reflectance spectra were taken by using a white-light source (tungsten iodine lamp) and the same detection apparatus as used in the PL measurements.

The characteristics of a microcavity can be calculated by using various methods [4, 9, 10]. Pavesi and co-workers have presented a calculation method for PSMs based on a combination of the quantum-box model with the TMM [11, 12]. As the light emission from PSi can be attributed to the quantum confinement effect [13], an exciton therein

will probably be confined in the silicon nanocrystal in a way analogous to an electron being confined in an isotropic dielectric cavity [14]. Thus, for a PSi layer containing pores of certain sizes, the dielectric function can be expressed as $\varepsilon(\omega) = \varepsilon_\infty + 4\pi\chi(\omega)$, where ε_∞, equal to n^2, is the background dielectric constant and $\chi(\omega)$ is the first-order resonant susceptibility which, in turn, is an integration over excitons of different frequencies resulting from different pore sizes. By selecting parameters properly and using the TTM relation $A + T + R = 1$ among reflectance (R), transmission (T) and absorption (A), various spectra of the PSMs can be obtained. The distribution of the electric field within a PSM can also be obtained in a similar way [15].

PSi is basically a mixture of silicon and air, so its refractive index should be lower than that of bulk Si, 3.4 [4], and should decrease with increasing porosity. The experimentally observed values are in the range from 1.3 to 2.2 for PSi prepared on heavily doped (∼0.01 Ω cm) p-type silicon wafers [7]. The Bruggeman effective medium approximation can be used to calculate also the average dielectric constant of each PSi layer [16]. It turns out that the stop-band of the DBR is not as wide as the emission spectrum (∼150 nm) of the PSi active layer. So, the light emission of the active layer in the cavity cannot be completely confined by the two Bragg mirrors, and leakage light may thus exist [17]. Furthermore, if the cavity resonant wavelength does not fall in the intensive emission region of the PSi active layer, the light emitting from the cavity may behave differently. There are three cases: namely, case I, the coincidence of the cavity resonant wavelength with the maximum of the active layer emission spectrum; and case II (case III), higher (lower) resonant wavelength than the peak wavelength of the PSi active layer. In the present calculation, the cavity resonant wavelength is tuned by changing layer thicknesses with refractive indices of all the layers remaining constant ($n_H = 2.1$, $n_L = 1.5$ and $n_{AC} = 1.3$). Matched optical thicknesses of the reflector layers and of the active layer are determined by the relations $n_H \times d_H = n_L \times d_L = \lambda/4$ and $n_{AC} \times d_{AC} = \lambda = 650$ nm, respectively.

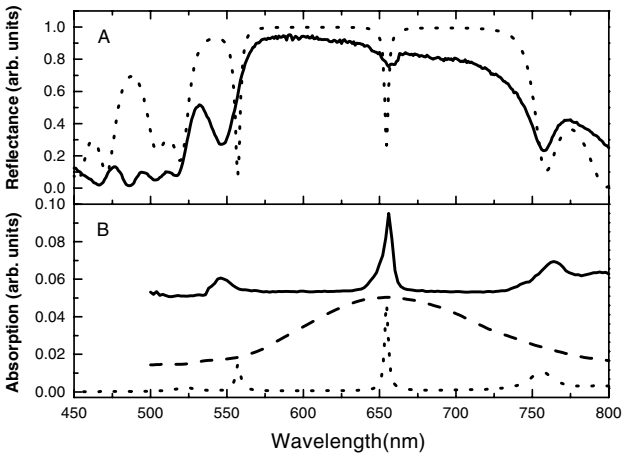

Figure 1. Calculated (dashed line) and measured (solid line) reflectance (A) and PL (B) spectra of a PSM sample in case I, where the cavity resonant wavelength coincides well with the maximum of the active layer emission spectrum. The measured PL spectrum of the active layer is also shown in (B) by the thick dashed line.

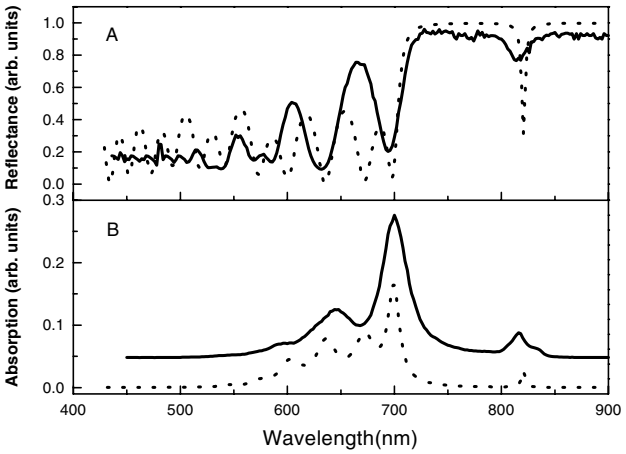

Figure 2. Calculated (dashed line) and measured (solid line) reflectance (A) and PL (B) spectra of a PSM sample in case II, where the stop-band of the DBR shifts to a higher wavelength.

3. Results and discussion

In order to give a good comparison between experimental and theoretical results, both measured (solid line) and calculated (dashed line) PL and reflectance spectra are shown in the same figures for the three different cases. Figure 1 shows the results of case I, where the cavity resonant wavelength (656 nm) coincides well with the maximum (661 nm) of the active layer emission spectrum. Thus, the light emitting from the PSM falls mainly in the central region of the stop-band and the full width at half maximum (FWHM) is measured to be 6 nm. Leakage light also appears at the low and high wavelength edges of the stop-band, due to the larger width of the emission spectrum from the PSi active layer than that of the stop-band. They are weak and broad because of the low emission intensity of the PSi active layer at the edges and the broad dip of the transmission maximum. As is immediately evident in the figure, the overall consistency between the calculated and measured spectra is quite good, except that the measured cavity dip is somewhat shallower and wider than that calculated. The discrepancy is probably due to the simplified model adopted for calculation that does not take into account influences of interface roughness, surface oxidation and dispersion of the light emitting from PSi [19].

When the stop-band of the Bragg mirrors shifts to higher wavelength (case II), the main peak in the emission spectrum emerges at the low wavelength edge of the stop-band rather than coinciding with the cavity mode itself, though the cavity resonance remains at the centre of the stop-band (figure 2). This is because the resonant wavelength of the cavity is longer than that of the PSi emission maximum. The main peak of the PL spectrum appears at a wavelength of 700 nm, though the cavity resonance dips at a wavelength of 816 nm. In this case, the dip of the transmission maximum at the low wavelength edge of the stop-band is close to the centre of the emission spectrum of the PSi active layer. The same characteristics can

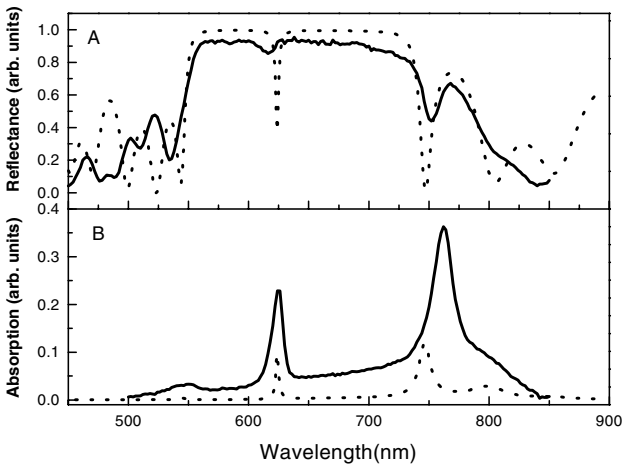

Figure 3. Calculated (dashed line) and measured (solid line) reflectance (*A*) and PL (*B*) spectra of a PSM sample in case III, where the stop-band of the DBR shifts to a lower wavelength.

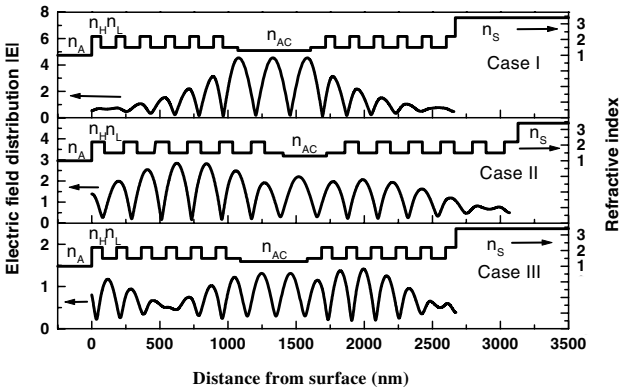

Figure 4. Calculated distribution of the electric field in the PSMs in the three cases. The upper curve in each panel is a scheme of refractive index variation in the PSM. The wavelengths of the main PL peaks, i.e. $\lambda = 656$ nm (case I), 700 nm (case II) and 762 nm (case III), are taken as the wavelengths of the incident light in the three cases, respectively. Symbols n_A, n_H (n_L) and n_S are the refractive indices of air, high (low) refractive index PSi layers and silicon substrate, respectively.

also be seen in the calculated spectra. In this case, several satellite peaks appear at wavelengths lower than that of the main PL peak of the microcavity, corresponding to the different transmission modes at the low wavelength edge of the stop-band. The flatness of the interface of the PSi layers determines the number of satellite peaks. So the emission spectrum in this case is characterized by the emergence of the main peak at the low wavelength edge of the stop-band accompanied by satellite peaks at lower wavelengths, in agreement with a recent report by Squire *et al* [20].

Alternatively, when the stop-band of the DBR shifts to a lower wavelength (case III), the main peak in the PL spectrum emerges at the high wavelength edge of the stop-band (figure 3). Due to the same reason as in case II, now the PSM emission peak and the cavity resonant wavelength appear at 762 nm and 624 nm, respectively. Similarly, satellite peaks appear at wavelengths higher than that of the main emission peak and the PL spectrum of this type of PSM is characterized by the emergence of the main emission peak at the high wavelength edge of the stop-band accompanied by satellite peaks at higher wavelengths.

Based on the above results of the three cases, we attribute the appearance of different reflectivity and PL spectra of PSi microcavities to the different wavelength positions of the stop-band of the DBRs and the broad emission light of PSi. Different characteristics of the three types of PSM can thus be considered as criteria to distinguish the PSMs from their PL spectra.

As further support to the above argument, figure 4 shows the calculated distribution of the electric field, normalized to the incident electric field, in the PSM of each of the three cases. The upper curve in each panel is a scheme of refractive index variation in the PSM. Symbols n_A, n_H (n_L) and n_S are the refractive indices of air, high (low) refractive index PSi layers and silicon substrate, respectively. The wavelengths of the main PL peaks, i.e. $\lambda = 656$ nm (case I), 700 nm (case II) and 762 nm (case III), are taken as the wavelengths of the incident light in the three cases, respectively. As one can clearly see in the figure, only in case I are the major electric field maxima confined in the active layer, with minor components penetrating into the adjacent mirror layers. In cases II and III, the electric field is now distributed over the whole system, and the major electric field maxima are not confined in the active layer, but shifted into the upper and lower mirror layers, respectively. This is why the main PL peak originating from the first transmission mode emerges at the low (high) wavelength edge of the stop-band in case II (case III).

The n_L value of 1.5 used in the present work corresponds to a PSi porosity of 70%, larger than the threshold of ∼45% for visible light emission [7]. This means that a single n_L layer itself can also be a source of light emission. The presence of the periodic n_H–n_L multilayer structure will narrow the emission, if any, as the stop-band of the DBR is not as wide as the emission from a single PSi layer. Narrow-line light emission also appears at the low wavelength edge of the stop-band, as shown in figure 5. The FWHM of the PL spectrum is 6 nm in the experiment. The theoretical reflectance and absorption spectra are in good agreement with the experimental results in both spectral shape and wavelength position. The inset in the lower panel of figure 5 shows the calculated distribution of the electric field in the PSi mirror, with the incident wavelength set at 600 nm, the wavelength of the main PL peak. One can see that the maxima are all located in the n_L layers, forming an amplitude oscillation in accordance with the n_H–n_L period. Such a phenomenon is basically the same as that predicted previously by Yariv and Yeh [21]. When the photon transferred is near the bandgap of the PSi medium, the threshold gain is much less than the loss. The nearer the bandgap, the lower the threshold gain. This is understandable, since the PSi layers with a lower refractive index emit light more efficiently and reabsorb the emitted light less due to a lower volume ratio of silicon [4]. The layered PSi structure is thus applicable to PSi lasers, in a way analogous to the use of artificially layered medium in a Bragg x-ray laser [21].

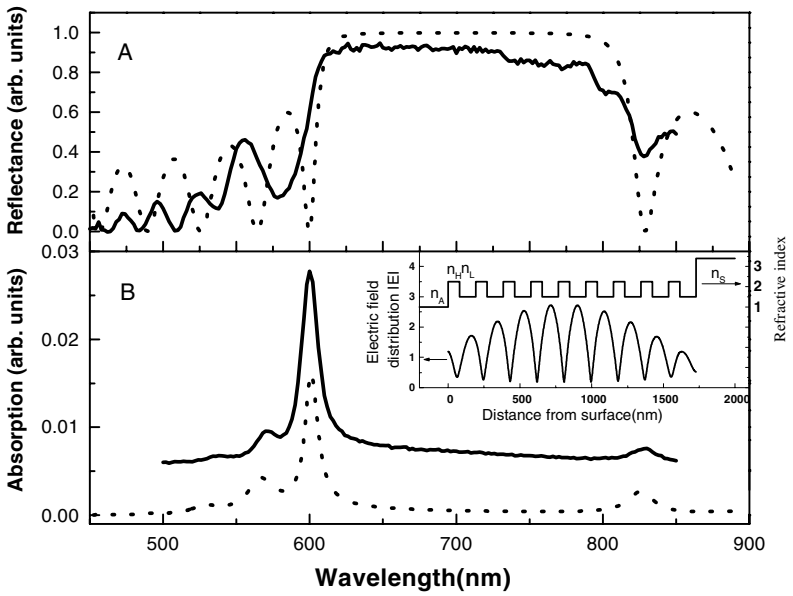

Figure 5. Calculated (dashed line) and measured (solid line) reflectance (*A*) and PL (*B*) spectra of a PSi DBR. The inset in (*B*) shows the electric field distribution in the PSi reflector. The incident wavelength is set at 600 nm, the wavelength of the main PL peak.

4. Conclusion

In this paper, we have presented a detailed study on PSi multilayers and microcavities prepared by the pulsed electrochemical etching method. Reflectivity and PL spectra were measured and compared with those calculated based on the TMM and quantum-box model. The great variety of reflectivity and PL spectra of the PSi microcavities can be attributed to the different positions of the stop-band of the DBRs and the broad light emission from PSi. The different characteristics of three types of PSM have been summed up. It is thus clear why PSMs may exhibit different light emission results and how the different confined field modes play their roles in the different cases of PSi microcavities. Future application of the PSi layered structure in PSi lasers may thus be expected.

Acknowledgment

This work was supported by National Natural Science Foundation of China, Ministry of Science and Technology under the 973 project, and Science and Technology Commission of Shanghai Municipality.

References

[1] Pavesi L, Mazzoleni C, Tredicucci A and Pellegrini V 1995 *Appl. Phys. Lett.* **67** 3280
[2] Xiong Z H, Yuan S, Jiang Z M, Qin J, Pei C W, Liao L S, Ding X M, Hou X Y and Wang Xun 1999 *J. Lumin.* **80** 137
[3] Chan S and Fauchet P M 1999 *Appl. Phys. Lett.* **75** 274
[4] Squire E K, Russell P St J and Snow P A 1998 *Appl. Opt.* **37** 7107
[5] Pavesi L, Guardini R and Mazzoleni C 1996 *Solid State Commun.* **97** 1051
[6] Hou X-Y *et al* 1996 *Appl. Phys. Lett.* **68** 2323
[7] Bisi O, Ossicini Stefano and Pavesi L 2000 *Surf. Sci. Rep.* **38** 1–126
[8] Xiong Z H, Liao L S, Ding X M, Xu S H, Liu Y, Gu L L, Tao F G, Lee S T and Hou X Y 2002 *Appl. Phys.* A **74** 807
[9] Lukosz W and Kunz R E 1977 *J. Opt. Soc. Am.* **67** 1607
Lukosz W 1979 *J. Opt. Soc. Am.* **69** 1495
[10] Benisty H, Stanley R and Mayer M 1977 *J. Opt. Soc. Am.* A **15** 1192
[11] Pellegrini V, Tredicucci A, Mazzoleni C and Pavesi L 1995 *Phys. Rev.* B **52** R14328
[12] Pavesi L, Panzarini G and Andreani L C 1998 *Phys. Rev.* B **58** 15792
[13] Canham L T 1990 *Appl. Phys. Lett.* **57** 1046
[14] Booker H G 1982 *Energy in Electromagnetism* (London: IEEE) p 57
[15] Zi J, Wan J and Zhang C 1998 *Appl. Phys. Lett.* **73** 2084
[16] Mazzoleni C and Pavesi L 1997 *Phys. Rev.* B **56** 15264
[17] Pavesi L and Pellegrini V 1999 *J. Lumin.* **80** 43
[18] Pavesi L and Dubos P 1997 *Semicond. Sci. Technol.* **12** 570
[19] Setzu S, Ferrand P and Romestain R 2000 *Mater. Sci. Eng.* B **69-70** 34
[20] Squire E K, Snow P A, Russell P St J, Canham L T, Simons A J and Reeves C L 1999 *J. Lumin.* **80** 125
[21] Yariv A and Yeh P 1977 *J. Opt. Soc. Am.* B **67** 438